

Aeration of surf zone breaking waves

Nobuhito Mori¹ and Satoshi Nakagawa²

¹ *Disaster Prevention Research Institute, Kyoto University, Gokasho, Uji 611-0011, Kyoto, Japan, E-mail: mori@oceanwave.jp*

² *Penta Ocean Construction Co. Ltd., 2-2-8 Koraku, Bunkyo-ku, Tokyo 112-8576, Japan*

Abstract. A set of laboratory experiments of the free surface elevation, the water velocity, the void fraction and the bubble distribution were conducted simultaneously for irregular wave breaking on a plane slope. The void fraction and bubbles induced by irregular wave breaking are different from regular wave case. It is, however, found that the relationship between the void fraction and the normalized turbulence intensity shows a linear dependence. In addition, the time-averaged void fraction can be estimated from the wave energy dissipation rate.

Key Words: surf zone, breaking wave, void fraction, energy dissipation

1. Introduction

Generally, the single phase flow approach to the ocean wave is successful for simulating wave transformation in the coastal area. However, waves steepen and break due to the bottom bathymetric effects in the near shore. The wave breaking create dense plumes of bubbles, and dissipates energy and momentum. An accurate estimate of bubble size and population distributions in the surf zone is important for understanding two-phase flow characteristics, solving engineering problems and environmental mechanisms of the coastal area (Donelan *et al.* 2002). The particularly oxygen transfer in shallow water region is important to avoid anoxia near urban coastal area. Recent photographic studies have illustrated the disintegration of entrapped air cavities divided into bubbles (Deane Stokes, 1999, 2002). However, there are unexplained aspects of the problem, such as enhanced bubble populations in salt rather than freshwater (Thorpe 1982), scale effects of void fraction and bubble size distribution in the laboratory experiments, and the relation between void fraction and turbulence.

Measurements of bubble size and population distributions, in-situ measurements (Chanson *et al.* 2002), video or photographic measurements (Leifer and de Leeuw 2002; Mori and Kakuno 2008) and acoustic measurements (Deane 1997) have been conducted. The bubble size measurements using lasers show high accuracy but are impossible to use in the presence of high void fractions due to

instrument limitations. Acoustic measurements of bubble are useful in deep-water but have limitation for very shallow water region due to the multi-reflection of sound beams. Therefore, conventional optical or resistivity type void probes are useful for surf zone waves. Vagle and Farmer (1998) compared four methods to measure bubble size and void fraction and showed that electrical conductivity probes should be used for the high void fractions.

Despite the fruitful knowledge of air entrainment for wind-wave breaking, few quantitative studies of air entrainment and of surf zone wave breaking exist. Loewen *et al.* (1996) found little difference in the bubble populations beneath mechanically generated surface waves in saltwater and freshwater. The compressibility due to air-water mixture decreases the velocity of sound and is being used to estimate large-scale prototype impacts, since the usual Froude scaling is unlikely to be correct for engineering problems. Therefore, the connection between air-mixture, bubble distribution and wave breaking induced turbulence is essential to understand the gas-liquid interaction in the surf zone. Cox and Shin (2003) and Mori *et al.* (2007a) reported on the dependence of void fraction on turbulent intensity in the bore region of surf zone waves. The wave breaking induced bubbles in the surf zone are split by strong local turbulent shear at the bubble scale (i.e. Deane and Stokes 1999). Rojas and Loewen (2010) measured the temporal and spatial variations of the void fraction fields beneath deep-water breaking waves by using a void fraction probe. They found that an energetic spilling breaker may entrain approximately the same volume of air as a steeper. However, qualitative and quantitative bubble characteristics in the surf zone and connections between bubble characteristics and wave breaking are not well known due to the lack of measurements in detail. This detail information of two-phase flow characteristics is required for mathematical modeling.

The purpose of this study is to investigate the characteristics of void fractions, bubble distributions and turbulent properties in the surf zone waves experimentally. First, a series of synchronized measurements of void fractions, bubble distributions, mean and turbulent components of flow above the mean water level in the surf zone are carried out for regular and irregular waves. Second, the analysis of the experimental data of void fractions, bubble spectra and turbulent properties of the surf zone waves, on onshore-offshore and vertical dependence of entrained air will be discussed.

2. Experimental setup

2.1 Method of Measurements

The purpose of this study is understanding the relation among air entrainment, bubbles size and liquid phase characteristics. If the instantaneous void fraction

exceeds 10%, the most reliable instruments are the intrusive phase detection probes in the laboratory (Mori *et al.* 2007a). In this study, dual-tip resistivity void probes (DVP) were developed in-house and used to measure high void fractions and large scale bubble size.

The needle type probe was originally developed by Neal and Bankoff (1965) and its design have since been refined by many researchers. The DVP used in this study consists of two stainless resistivity void probes and measures the electric voltage change of the probes. The diameter of the probe is 0.12 mm and the head was sharpened to an angle of 21 degrees. Each probe was insulated except at the head. Two probes are combined into one and these heads were shifted 0.5 mm - 1.0 mm to detect the phase shift of voltage change. The direct individual bubble event analysis has reliability and robustness under the strong turbulent flows. Therefore, we adopt individual bubble analysis method in here.

The basic principal and calibration of DVP are summarized as follows. We define the distance Y between two heads. The distance Y can be measured by microscope. If a bubble penetrates the DVP, the velocity of the bubble moving at speed v_b can be estimated by the time lag between two heads

$$v_b = \frac{Y}{\Delta t_s}, \quad (1)$$

where Δt_s is the time lag, Y is the head distance between two tips. The distance of probe heads Y should be larger than characteristic space length of the bubbly flow and be smaller than mean bubble diameter (Hibiki *et al.* 1998)

$$\frac{N_s v}{f} \leq Y \leq d_m, \quad (2)$$

where N_s is the number of sampling points for one bubble, f is the sampling frequency of data, d_m is the mean bubble chord length. Generally, the sampling frequency is 5k-50kHz and should be small enough but minimum resolution also depends on physical sensor size. The conversion from the bubble chord length to the diameter was followed by Monte-Carlo simulation developed by Mori *et al.* (2007a).

On the other hand, the instantaneous void fraction $\alpha(x, z, t)$ can be calculated by the small time duration of wetting/drying time ratio at the tip.

$$\alpha(x, z, t) = \frac{\sum_t^{t+\Delta t} t_g^i}{\sum_t^t t_l^i} \quad (3)$$

where t_g^i is the drying time of the tip and t_l^i is the time of tip in the liquid. The probe

was located above the free surface for wave crest measurements and the data during outside of water were removed using wave gauge data. For long-time integration of the recorded data, Eq.(3) becomes the time-averaged void fraction, $\bar{\alpha}(x, y)$. If the integration time length Δt is enough smaller than the wave period, the void fraction defined by Eq.(3) can be regarded as instantaneous or short time-averaged void fraction. The probe response depends on the wetting and drying time of the tip, and response time of the probe and electronics. Thus, the response time of the probe was calibrated, using a calibration system. The accurate threshold value of voltage change of the DVP for the air-water interface was determined comparing V and v_b .

The instantaneous water velocity was measure by acoustic Doppler velocimeter (ADV, Sontek). The sampling frequency of the ADV was 200Hz. ADV recorded data included spike noise due to the Doppler signal aliasing, air bubble effects and so on (*i.e.* Voulgaris and Trowbridge 1998; Elgar *et al.* 2001). A major problem is that the spike noise looks similar to turbulent components in the velocity data. Therefore, several despiking algorithms have been proposed to remove spike noise from ADV recorded velocity data. Generally, Fourier low-pass filtering, moving averaging, and acceleration threshold (first differential of velocity) methods are used for removing spiking noises from ADV data. The 3D phase space method proposed by Goring and Nikora (2002) is an excellent method despiking of ADV data due to the efficiency and no requirement for empirical coefficients. The modification of the 3D phase space method was evaluated by Wahl (2003) and application of it to bubbly flow was investigated by Mori *et al.* (2007a). We use the true 3D phase space method with correlation and SNR filter to exclude spike noise from raw data.

2.2 Experimental Setup

A set of experiments were conducted using a two dimensional wave flume (1.0 m wide, 1.5 m high and 50.0 m long). A fixed, impermeable 1/30 slope was installed with the toe 20 meters from the wave-maker. The water depth was 0.8 m, and both regular and irregular wave trains were generated by a PC controlled wave-maker with an active wave absorber.

The water surface elevation, water velocities, void fractions and bubble chord length distributions were measured by a movable array mounted with a wave gauge, an ADV and a DVP (see Figure 1). Assuming statistical homogeneity in the alongshore direction, the wave probe, DVP and ADV were mounted at the same location from the shoreline (x direction) in alongshore direction. A detail of the experimental setup is shown in Figure 1 where x is the horizontal coordinate to shoreline, y is the horizontal coordinate perpendicular to x , and z is the vertical

coordinate respectively. The wave gauge, ADV and the DVP were sampled at 100 Hz, 200 Hz, and 5 kHz, respectively. All sensors were synchronized by TTL signal from the wave maker. The measurements were traversed horizontally 12-20 points with 4 cm interval from wave breaking point (B.P.) to shoreline and vertically 10-12 points with 1-2 cm interval depends on the wave height and local water depth. The measurements locations were mainly selected near the water surface where is highly aerated region due to wave breaking. For each trial, measurements were conducted for 5 minutes to establish equilibrium conditions of breaker position. Data were recorded at each locations for at least 100 waves minimumly.

The only data of ADV and DVP in the liquid phase were analyzed based on the synchronized signal from the wave probe. As mentioned in the previous section, the measured ADV data were filtered by the 3D phase space method (Wahl 2003; Mori *et al.* 2007b).

2.3 Regular wave condition

The regular wave experiments were conducted by two different breaking wave condition as shown in Table 1. The two cases of regular waves were run,

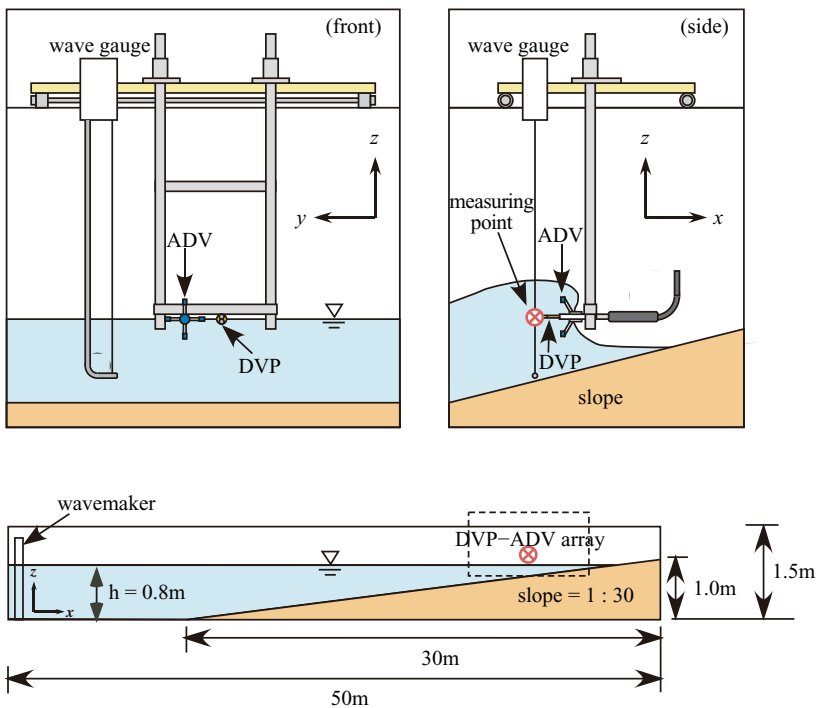


Figure 1 Illustration of the experimental setup

Table 1 Regular wave condition

case	Type	T [s]	H_0 [cm]	L_0 [m]	H_b [cm]	h_b [cm]	X_s [m]	ξ_0
1-reg	spilling	1.6	16.3	3.55	19.4	21.7	6.5	0.16
2-reg	spilling/plunging	2.0	11.5	4.85	13.5	13.0	3.9	0.22

Table 2 Irregular wave condition

case	spectrum	$T_{1/3}$ [s]	$H_{1/3}$ [cm]	η_{rms} [cm]	f_p [1/s]
1-irrB	Bretschneider-Mitsuyasu	1.6	23.1	5.76	0.63
1-irrJ	JONSWAP	1.6	23.1	5.76	0.63
2-irrB	Bretschneider-Mitsuyasu	2.0	16.3	4.07	0.50
2-irrJ	JONSWAP	2.0	16.3	4.07	0.50

characterized by their breaking type to give spilling (Case 1), spilling/plunging (Case 2). Table 1 summaries the wave statistics for Case 1 and 2 where T is the wave period, H_0 is the deep-water wave height, H_b is the breaking wave height at the breaking point (B.P.), h_b is the water depth at the breaking point, and X_s is the length of the surf zone. The notation ξ_0 ($=h_x/\sqrt{H_0/L_0}$) in the table indicates the surf similarity parameter and the first case is spilling breaking condition and the second case is the intermediate between spilling and plunging wave condition.

2.4 Irregular wave condition

The irregular wave experiments were conducted by two different breaking heights and spectra as shown in Table 2. The wave heights were equivalent to the regular wave condition in the energy level as shown in Table 1 ($H_{1/3} \approx 1.416H_0$), although the wave periods were similar to the regular wave condition. The notations $H_{1/3}$, $T_{1/3}$, η_{rms} and f_p are significant wave heights, significant wave periods, rms values of the surface elevation and peak frequencies of spectra in offshore, respectively. The two different wave spectra of Bretschneider-Mitsuyasu and JONSWAP are given for the same wave height condition. Following the results of regular and preliminary experiments, horizontal and vertical distributions of measurements were conducted from the starting point of wave height attenuation due to shallow water breaking effects. Comparing with the regular and irregular wave experiments, it is possible to check the sensitivity of the void fraction and its spatial distributions to the wave conditions.

3. Results and discussions

It is useful to examine relationship between onshore-offshore distributions of

wave field and void fraction. Figure 2 indicates a series of horizontal distribution related to breaking wave characteristics. The panels in each figure show mean wave heights, time-averaged void fractions $\bar{\alpha}(x, z)$, bubble number densities N and mean chord lengths d_m from the breaking point (B.P.) to shoreline, respectively. The horizontal distribution of the time-averaged void fraction at the mean water level (MWL) $\bar{\alpha}(x, 0)$ shown in panels (i) gives a characteristic profile in comparison with wave height decay from B.P. For example, the time-averaged void fraction $\bar{\alpha}(x, 0)$ in Figure 2 (i), the regular wave case, is monotonically increased from B.P. and is reached at maximum value. The maximum value is continued about one wave length and is gradually decreased after that. The highly saturated void fraction region is started from the 1st plunging point to the near shore. On the other hand, there is no significant peak of $\bar{\alpha}(x, 0)$ for the irregular wave case in Figure 2 (ii). The time-averaged void fraction of the irregular waves is less than half of the void fraction of regular waves with the same incident wave energy. In addition, the time-averaged void fraction of the irregular wave case is less than half of regular wave case for the same wave energy condition. There is no clear wave spectrum dependence of the void fraction but the differences between regular and irregular are significantly large. The differences of the void fraction between the regular and irregular are basically due to different wave breaking mechanisms and the irregular location of the B.P. There is a clear B.P. in the case of regular waves and the wave height rapidly decreases after the first plunging point. Therefore, the void fraction has a clear peak after the B.P. in the case of regular waves. On the other hand, the wave breaking is spatially and temporally sparse for irregular waves. Thus, the both wave height attenuation and related the void fraction gradually decreased.

The injected bulk of air is divided by shear flows due to wave breaking induced turbulence. On the other hand, the entrapped air induced by wave breaking generates strong turbulence near the free surface. Cox and Shin (2003) reported the dependence of void fraction on turbulent intensity in the bore region of surf zone waves. The synchronized observations of void fraction and turbulence for the breaking waves were conducted in this study. Therefore, the relationship between the void fraction and turbulence will be examined hereafter.

The turbulence component in onshore-offshore direction σ_x is used as characteristic turbulence intensity in here. The total turbulent kinetic energy is also similar but the turbulence component in principal direction is only considered for simplicity. Figure 3 shows relation between the time-average void fraction $\bar{\alpha}(x, z)$ and σ_x . The turbulence component is normalized by \sqrt{gh} at the measurement location. Overall, the relationship between the time-averaged void fraction and turbulence intensity is clear. The correlation coefficient is 0.92. More than 10% of

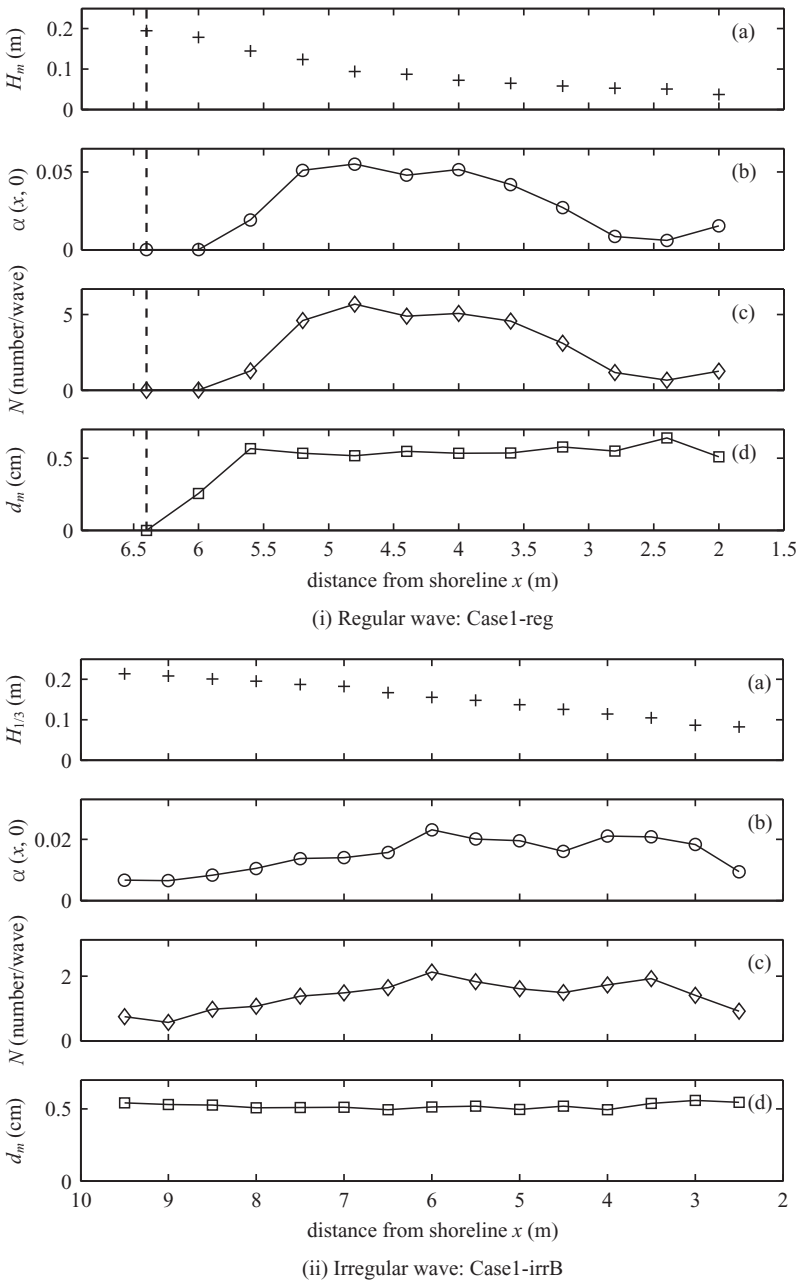


Figure 2 Onshore-offshore distribution of wave and bubble statistics at mean water level (MWL) (a) Mean wave height H_m and $H_{1/3}$, (b) void fraction $\alpha(x, 0)$, (c) number of bubbles per wave, (d) mean bubble length d_m)

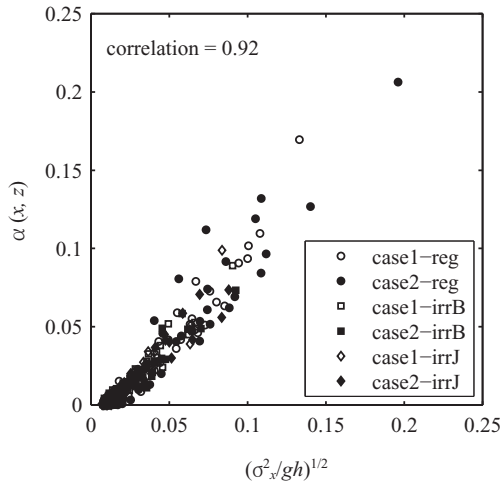


Figure 3 Relation between the time-average void fraction $\bar{\alpha}(x, z)$ and the square of turbulent intensity to x direction σ_x^2

turbulence component σ_x with respect to characteristic mean flow velocity in the shallow water, \sqrt{gh} , in the surf zone corresponds to 10% of bubbly flow. There is no significant difference between the regular and irregular waves and locations in the surf zone. The similar analysis for the regular waves was given by Cox and Shin (2003) and previous our study (Mori *et al.* 2008) but this is first results for irregular wave cases.

The relation between the local void fraction and turbulence components are implicit. The existence of bubble enhances surrounded turbulence and turbulence shear splits the bubble. For low void fraction case, however, one-way interaction from liquid to air phase can be assumed. Based on this result, the time-averaged void fraction can be estimated by the liquid phase turbulence component neglecting aeration enhance turbulent flow. The further theoretical consideration will be required finding the universal relationship between the turbulence characteristics of breaking wave and void fraction.

In the context of bubble generation, wave breaking induced turbulence in the surf zone is strongly related to wave energy dissipation. The wave breaking decreases the wave energy and the intensity of turbulence components is related to the void fraction. Therefore, the wave dissipation can be regarded as a direct indicator of two phase flow characteristic in the surf zone. There are many wave height dissipation models which have been verified in detail. Guza and Thornton (1983) formulated the depth-averaged wave energy dissipation rate ϵ for surf zone breaking waves as

$$\varepsilon = -\frac{1}{8} \frac{g}{h} \frac{d(c_g H_{rms}^2)}{dx} \quad (4)$$

where ε is the vertically averaged wave energy dissipation rate per unit volume, c_g is the group velocity, g is the gravity acceleration and H_{rms} is the root-mean-square value of the wave height. The horizontal distribution of ε at the MWL can be estimated by the observed wave height decay as shown in Figure 2.

The estimated wave energy dissipation rate by Eq.(4) shows similar to the void fraction (not shown in figure). Figure 4 shows the relationship between ε and $\bar{\alpha}$. The correlation between ε and $\bar{\alpha}$ is 0.89 but their relation is not linear for larger values of ε . This relation between the wave energy dissipation rate and time-averaged void fraction is pretty useful because the wave energy dissipation rate can be directly computed from the wave equation such as Boussinesque equation.

4. Conclusions

Using the two-phase flow measurement array, the characteristics of void fractions, air bubble distributions, and flow velocities were measured for surf zone breaking waves in the laboratory. Both regular and irregular wave experiments were conducted to measure void fraction and bubble size spectra. The results of this study can be summarized as a expansion of previous studies as follows.

1) The relationship between the time-averaged void fraction and the intensity of

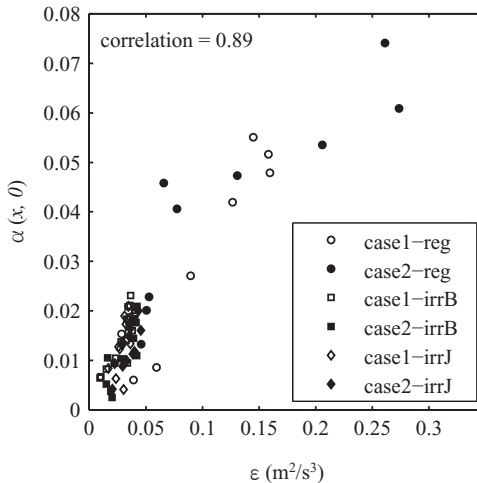


Figure 4 Relation between time-averaged void fraction $\bar{\alpha}(x, 0)$ at mean water level (MWL) and wave energy dissipation rate ε

turbulence shows a linear dependence.

- 2) The time-averaged void fraction can be estimated from the wave energy dissipation rate.

The unsteady characteristics of two-phase flow in the surf zone are important, although the time-averaged characteristics were analyzed in this study.

Further studies on the temporal characteristics will be required.

Acknowledgements

The authors express grateful thanks to Professor Shohachi Kakuno who had passed away December, 2009. This research was funded by the Ministry of Education, Science, Sports and Culture, Japan, through Grant-in-Aid and DPRI, Kyoto University research fund.

References

- Chanson, H., S. Aoki, and M. Maruyama (2002). Unsteady air bubble entrainment and detrainment at plunging breaker: Dominant time scales and similarity of water level variation. *Coastal Engineering* 46, 139–157.
- Cox, D. and S. Shin (2003). Laboratory measurements of void fraction and turbulence in the bore region of surf zone waves. *Journal of Engineering Mechanics, ASCE* 129(10), 1197–1205.
- Deane, G. B. (1997). Sound generation and air entrainment by breaking wave in the surf zone. *J. Acoustic Soc. America* 102, 2671–2689.
- Deane, G. B. and M. D. Stokes (1999). Air entrainment processes and bubble size distributions in the surf zone. *Journal of Physical Oceanography* 29, 1393–1403.
- Deane, G. B. and M. D. Stokes (2002). Scale dependence of bubble creation mechanisms in breaking waves. *Nature* 418, 839–844.
- Donelan, M., W. Drennan, E. Saltzman, and R. Wanninkhof (2002). *Gas Transfer at Water Surfaces*. Washington DC: AGU.
- Elgar, S., B. Raubenheimer, and R. Guza (2001). Current meter performance in the surfzone. *J. Atmospheric and Ocean Technology* 18, 1735–1746
- Goring, D. G. and V. I. Nikora (2002). Despiking acoustic Doppler velocimeter data. *Journal of Hydraulic Engineering* 128(1), 117–126.
- Guza, R. and E. Thornton (1983). Velocity moments in nearshore. *Journal of Waterway, Port, Coastal, and Ocean Engineering* 111(2), 235–256.
- Hibiki, T., S. Hogsett, and M. Ishii (1998). Local measurement of interfacial area, interfacial velocity and liquid turbulence in two-phase flow. *Nuclear Engineering and Design* 184, 287–304.
- Leifer, I. and G. de Leeuw (2002). Bubble measurements in breaking-wave generated bubble plumes during the LUMINY wind-wave experiment. In M. Donelan, W. Drennan, E. Saltzman, and R. Wanninkhof (Eds.), *Gas Transfer at Water Surfaces*, pp. 303–310. Washington DC: AGU.
- Loewen, M., M. O’Dor, and M. Skafel (1996). Bubbles entrained by mechanically generated breaking waves. *Journal of Geophysical Research* 101, 20759–20769.
- Mori, N. and S. Kakuno (2008). Aeration and bubble measurements of coastal breaking

- waves. *Fluid Dynamics Research* 40(7-8), 616–626.
- Mori, N., T. Suzuki, and S. Kakuno (2007a). Experimental study of air bubbles and turbulence characteristics in the surf zone. *Journal of Geophysical Research* 112 (C05014), doi:10.1029/2006JC003647.
- Mori, N., T. Suzuki, and S. Kakuno (2007b). Noise of acoustic Doppler velocimeter in bubbly flow. *Journal of Engineering Mechanics* 133(1), 122–125.
- Neal, L. G. and S. G. Bankoff (1965). Local parameters in cocurrent mercury-nitrogen flow. *Am. Inst. Chem. Journal* 11, 624–635.
- Rojas, G. and M. Loewen (2010). Void fraction measurements beneath plunging and spilling breaking waves. *Journal of Geophysical Research* 115(C8), C08001.
- Thorpe, S. (1982). On the clouds of bubbles formed by breaking wind waves in deep water, and their role in air-sea gas transfer. *Phil. Trans Roy. Soc. Lond.* A304, 155–210.
- Vagle, S. and D. Farmer (1998). A comparison of four methods of bubble measurement. *IEEE Oceanic Engineering* 23(3), 211–222.
- Voulgaris, G. and J. H. Trowbridge (1998). Evaluation of the acoustic doppler velocimeter (ADV) for turbulence measurements. *Journal of Atmospheric and Oceanic Technology* 15(1), 272–289.
- Wahl, T. L. (2003). Discussion of “Despiking acoustic Doppler velocimeter data”. *Journal of Hydraulic Engineering* 129(6), 484–488.